THE Catalyst at UC San Diego
https://catalyst-research.ucsd.edu

Volume 2
Sep 30, 2024

Robust Design and Optimization of Turbo-machinery Compressors

by Preston Gomersall, Devanshi Jain
edited by Jennifer Fromm
doi:10.57949/C9H59Z

Gomersall, P., & Jain, D. (2024) Robust Design and Optimization of Turbo-machinery Compressors. The Catalyst at UCSD, 2, 32-51.
https://doi.org/10.57949/C9H59Z

Robust Design and Optimization of Turbo-machinery Compressors

Preston Gomersall & Devanshi Jain

Abstract

This research is dedicated to advancing gas turbine technology for greener and more cost-effective commercial air transportation. The focus lies in optimizing the High Pressure Compressor (HPC) component of NASA's Energy Efficient Engine (EEE) which compresses air prior to entering the combustion chamber. The goal for the research project was to improve the compressor's pressure ratio from inlet to outlet to enhance the efficiency of the combustion process. Factors affecting compressor performance, such as blade twist angle, blade geometry, and shroud and hub tip clearance, are analyzed and optimized to improve efficiency and overall performance. Computational Fluid Dynamics (CFD) models were created within the Ansys software suite and successfully optimized by leveraging the San Diego Supercomputer Center. This research achieved a pressure ratio increase across the first four stages of a ten-stage compressor, surpassing NASA's 1980 model. This paper outlines the methodology, including geometry generation using Ansys BladeModeler, blade row meshing with TurboGrid, and CFX (Fluid dynamics) simulations. The optimization process involved multiple design iterations and a response surface method to attain the highest pressure ratio. The multidisciplinary approach underscores the potential of leveraging emerging technologies of CFD and High Performance Computing to significantly improve the efficiency of existing models, as exemplified by the successful optimization of the EEE's HPC.

Nomenclature

BPR	ByPass Ratio	**LPC**	Low Pressure Compressor
CAD	Computer Aided Design	**LPT**	Low Pressure Turbine
EEE	Energy Efficient Engine	$\mathbf{N_C}$	Corrected Rotational Speed
HPC	High Pressure Compressor	**NLH**	Non-Linear Harmonic
HPT	High Pressure Turbine	**NPSS**	Numerical Propulsion System Simulator
ICLS	Integrated Core Low Spool		

Introduction

Over the past decade, substantial attention and dedicated research has been directed towards enhancing the efficiency of gas turbine engines. Notably, the aviation sector is responsible for contributing approximately 2.8 percent of the total global greenhouse gas emissions[6]. Presently, airlines are engaged in progressive endeavors involving the exploration of natural oils and novel fuel compositions, all aimed at mitigating the impact of greenhouse gas emissions. Concurrently, innovative initiatives are underway, involving the experimentation with advanced blade materials, exemplified by the utilization of cutting-edge carbon fiber composites[7]. This particular carbon fiber technology has the capacity to withstand elevated temperatures and more formidable mechanical stresses.

In alignment with these industry-wide aspirations, our project undertakes a distinct focus on the meticulous selection of optimal geometries, blade counts, as well as the intricacies of hub and shroud curves, with the ultimate aim of refining fluid dynamics through a compressor. Our project utilizes the foundational geometry derived from NASA's Energy Efficient Engine (EEE) project, a publicly accessible blueprint originating from the pioneering work conducted during the 1980s at the NASA Glenn Research Center[1]. Computational fluid dynamics, which are computer simulations of how fluids flow, have drastically improved in the last decade. Our plan is to use these improvements to make the EEE model even more efficient.

Background

In order to gain a comprehensive grasp of this paper, it is imperative to have foundational knowledge about turbofan and turbojet engines. A fundamental depiction of the core of a turbojet engine is illustrated in Figure 1. The thermodynamic cycle that air undergoes within a turbojet engine involves a sequential progression through compression, combustion, and turbine stages, culminating in the converging-diverging nozzle.

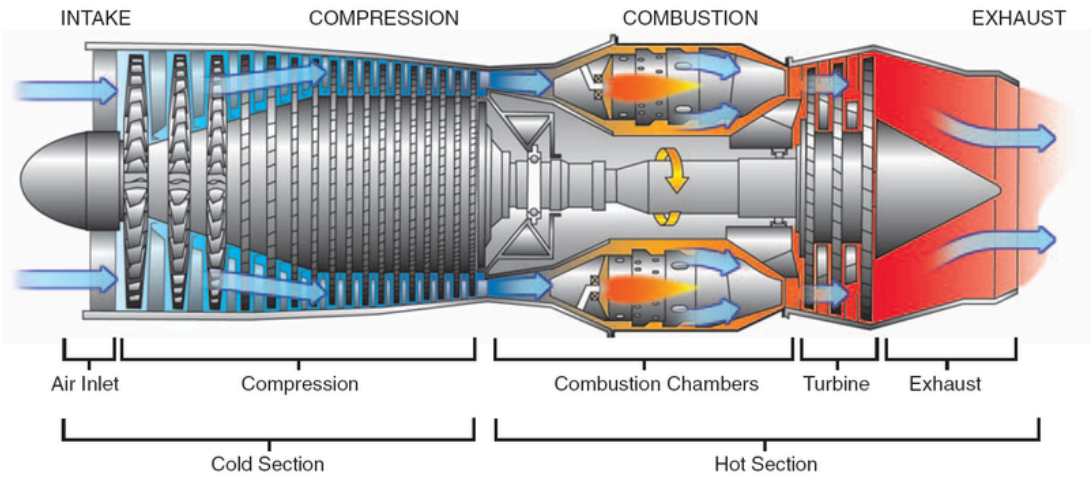

Fig. 1 The core of a jet engine[8].

The process begins with the compression of air, a vital preparation for subsequent combustion. Optimal combustion transpires at elevated pressures and temperatures, facilitating superior fuel-air mixing and heightened reaction rates. The mixing of compressed air with fuel is followed by ignition through a spark, yielding thermal energy. This thermal energy is transformed into kinetic energy, inducing turbine rotation and propelling air rearward to produce thrust for the aircraft.

For this project a turbofan engine was modeled which can be seen in Figure 2. Turbofan engines have low and high pass compressors and turbines because the engines are split into two sections. The first section being the air pathway that goes through the core of the engine and the second being the air pathway that travels around the perimeter of the engine. The ratio between the amount of air that travels through the core to the amount of air that travels around the exterior is called the ByPass Ratio (BPR). The BPR has a significant effect on the engine's efficiency[2].

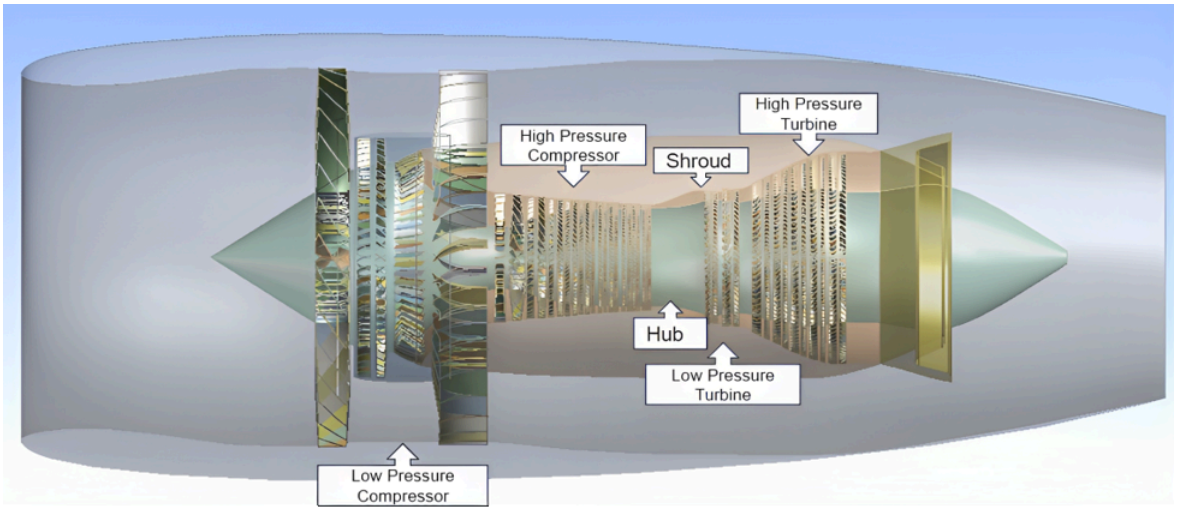

Fig. 2 Final updated geometry of the Energy Efficient Engine.

Methodology

1. System Description

Our methodology involves the development of a turbofan geometry and the simulation of the engine's performance under cruise flight conditions at 35,000 feet and a flight speed of MACH 0.8. A pivotal aspect of our approach involves the utilization of Computational Fluid Dynamics (CFD) analysis, which enables us to delve into the intricate interactions of fluid flow within the compressor blades of turbojet engines.

Among various options in CFD simulation software, Ansys stood out for its accuracy, efficiency, and comprehensive functionalities in meshing turbine blades and approximating the flow conditions at each point along the compressor. These attributes position Ansys as an optimal fit for the intricate task of turbojet engine optimization. The decision to employ Ansys expedites our design through an analysis pipeline, enabling us to achieve efficient designs with a more streamlined approach.

2. Pre Processing

2.1 Process Overview

First we will give a brief summary of the entire process as depicted in Figure 3. The process begins by creating a meticulously designed geometry using Ansys DesignModeler. This geometry is then transformed into a surface mesh using the TurboGrid tool. Following this step, our focus shifts to CFX, where we set up the input and boundary conditions. The subsequent stages involve solving equations that define fluid flow such as the Navier-Stokes flow equations and analyzing the outcomes using CFD-Post.

Our approach delves further by encompassing a spectrum of input and output parameters within the domain of Response Surface Optimization (RSO). Through this iterative cycle, we refine modified geometries, construct meshes, and evaluate these adjusted design points. This iterative progression guides us in identifying optimal geometry configurations —ones that excel in enhancing the pressure ratio across each stage of the axial compressor.
This encapsulates a workflow that transitions through different steps, integrating design, analysis, and optimization. The aim is to uncover the most effective configurations for enhancing the pressure ratio across the intricate arrangement of rotor-stator stages within the axial compressor.

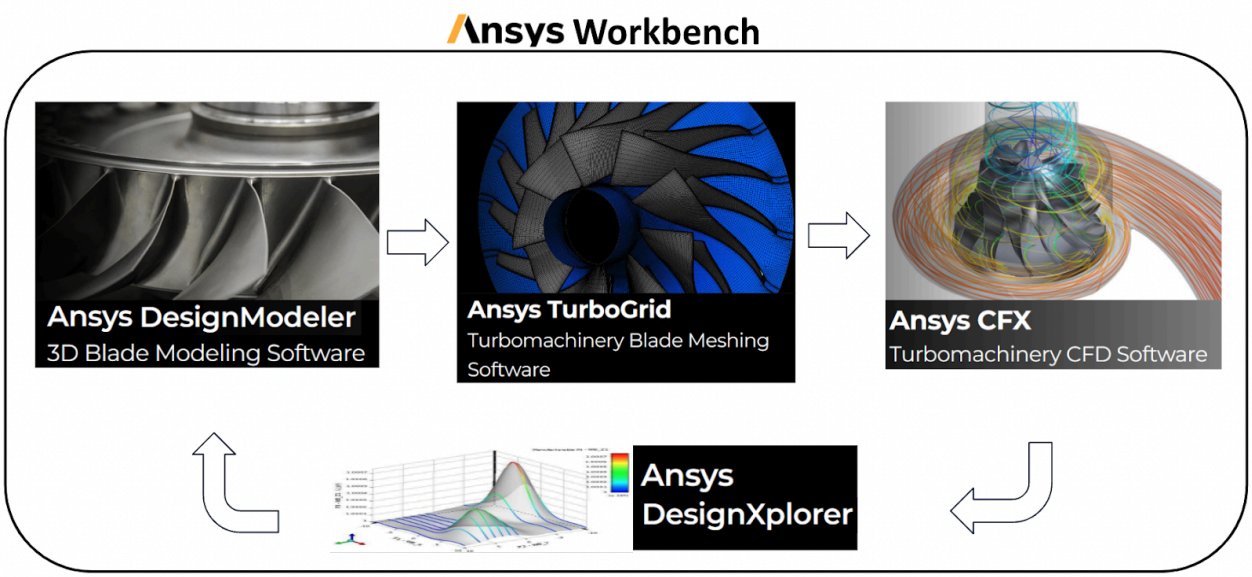

Fig. 3 Workflow set-up within Ansys Workbench using a suite of Ansys' turbomachinery tools.

2.2 Geometry Modeling

Instead of creating the geometry of the axial compressor from scratch we utilized the NASA EEE[3] engine as our default geometry. Upon importing the geometry, we obtain the configuration depicted in Figure 4. This marks the initial setup within Ansys Design Modeler, encompassing 21 blades including the Inlet Guide Vane, followed by 10 subsequent stages of rotors and stators. To precisely define the geometry for each blade row in the engine, including the Low Pressure Compressor (LPC), High Pressure Compressor (HPC), High Pressure Turbine (HPT), and Low Pressure Turbine (LPT), we draw upon circumferential blade count data from Table in 1 which is provided in the same NASA paper[3].

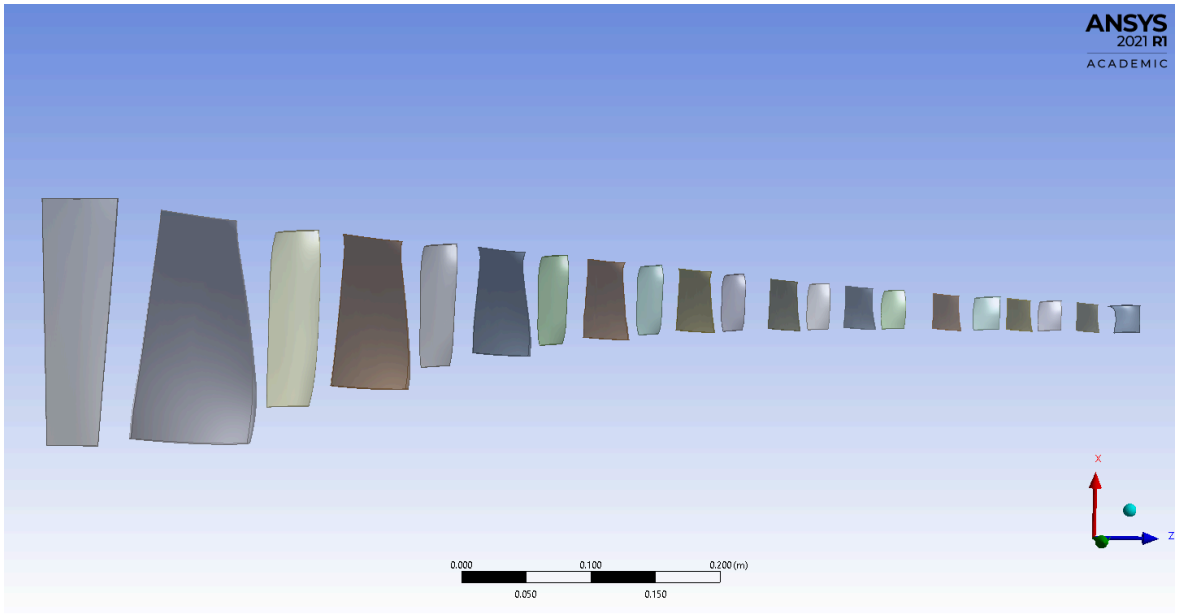

Fig. 4 Workflow set-up within Ansys Workbench using a suite of Ansys' turbomachinery tools.

To prepare the geometry for simulation we created blades rows around the axial line of the engine, resulting in the intricate geometry portrayed in Figure 5b. This initial geometry exhibits striking parallels with the schematic of the General Electric's EEE shown in Figure 5a . The sequence portrays a distinct progression: commencing with the initial configuration of the Inlet Guide Vane, rotor, and stator blades, advancing through the integration of circumferential blade count data, and culminating in the comprehensive initial geometry of the turbojet engine.

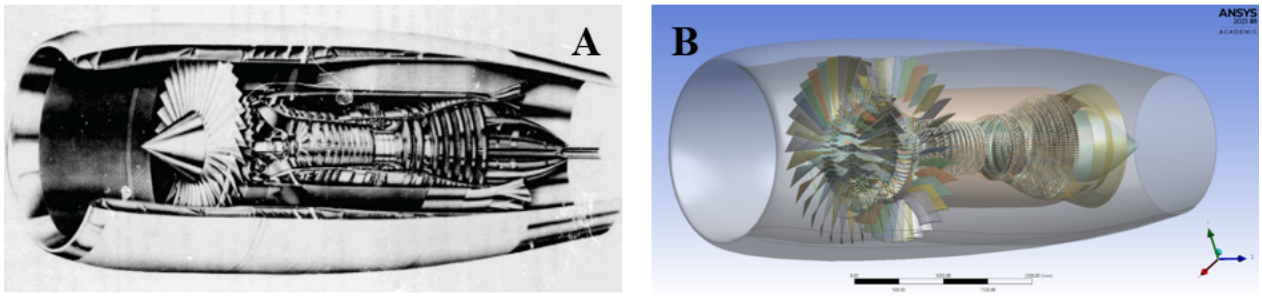

Fig. 5 Physical and Computational Model of the Energy Efficient Engine. **A** Energy Efficient Engine developed by General Electric. **B** Complete initial setup of turbojet geometry.

Following the establishment of the overall turbojet engine setup, our attention shifts to extracting the geometry of the axial compressor—a pivotal turbomachinery component central to our research. The axial compressor holds a critical role in increasing the pressure of incoming air, significantly influencing the engine's overall performance.

Within the axial compressor, three components assume distinct roles in facilitating the

compression process for a 10-stage configuration, as elucidated by Figure 6A:

Inlet Guide Vane (IGV): Positioned at the forefront of the compressor, the IGV functions as a vital air guide. Its primary task is to direct the incoming airflow, ensuring an optimized Angle of Attack (AOA) into the subsequent rotor stages. This strategic guidance lays the foundation for an efficient and seamless transition throughout the compression process.

Rotors: These dynamic components, securely affixed to the hub or inner layer, play a decisive role in the compression journey. By propelling the air with heightened velocity, rotors induce a crucial increase in its kinetic energy. This enhanced velocity sets the stage for the subsequent phases of compression.

Stators: In contrast, stators are stationary and are fixed to the shroud or outer casing. Stators guide and slow the airflow, increasing the pressure. This deceleration is vital to prevent backflow and surge.

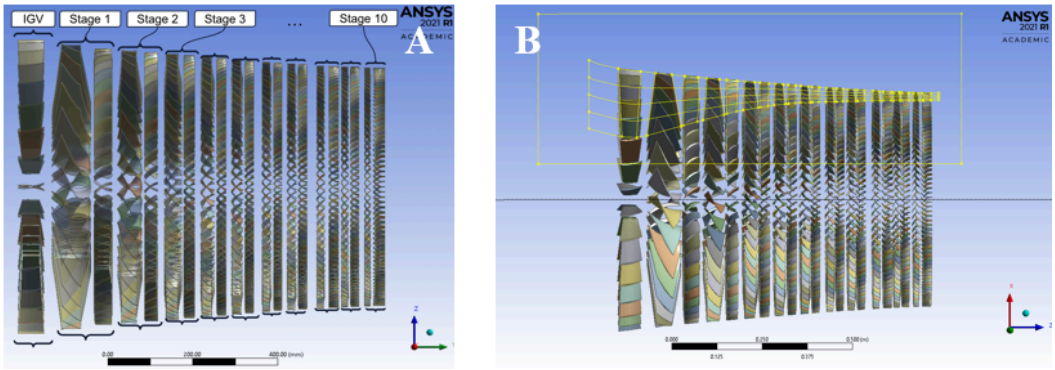

Fig. 6 **A** Extracted 10-stage Compressor Geometry. **B** Flowpath Implementation on Compressor.

2.3 Mesh Generation

We generated high-quality blade passage meshes within axial compressors using Ansys TurboGrid[4]. These blade meshes, as shown in Figure 7, are pivotal for accurately simulating complex fluid dynamics and interactions between rotor and stator components. This section details the process of generating high-quality meshes, a crucial step for ensuring accurate and reliable simulations.

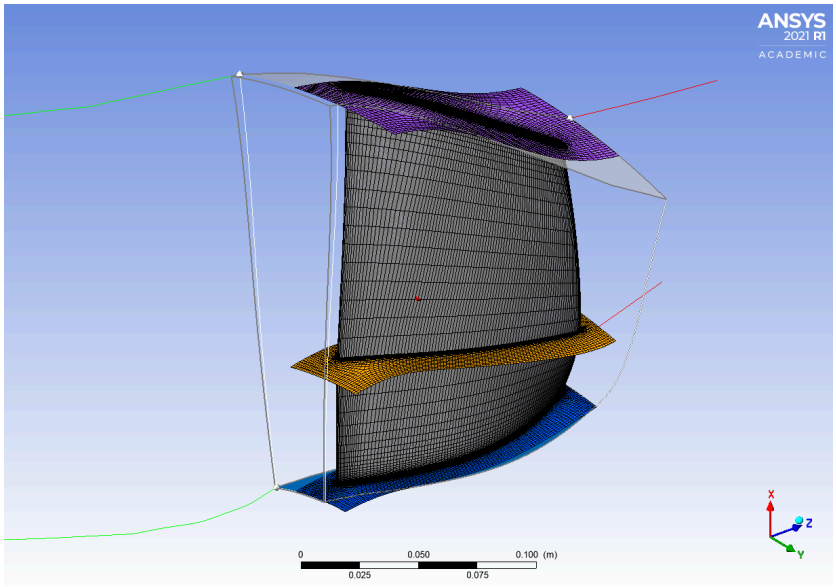

Fig. 7 Blade Mesh.

To begin, the flow path within the rotating machine is divided into specific volumes, as shown in Figure 7. We primarily use hexahedral elements for a structured and uniform mesh, crucial for capturing the complex fluid dynamics within the axial compressor. At the blade tip, we introduce wedge elements to accurately model geometric intricacies. The union of these elements forms a comprehensive mesh that serves as input for the Ansys CFX solver, driving our simulations. The quality of this mesh is critical, directly affecting the accuracy and reliability of our simulation results, enabling precise predictions and optimizations in blade design.

Mesh Optimization: We address potential gaps, particularly around the blade tips, using predictive models to foresee their impact on airflow. This strategy allows us to optimize the mesh without excessive refinement, maintaining computational efficiency. The dynamically adjusted mesh based on the solution and geometry ensures our simulations remain within 5% of actual values, validating our research findings.

Mesh Quality Analysis: To ensure mesh quality, we analyze key parameters such as Minimum Face Angle, Maximum Face Angle, Element Volume Ratio, Edge Length Ratio, and Connectivity Number, as detailed in Table 1. This rigorous analysis guarantees that the mesh meets strict quality standards essential for reliable simulations. Ansys TurboGrid efficiently computes the topology and refined mesh for both hub and shroud layers. The topology, shown with dark pink lines in Figure 10, guides the creation of the refined mesh, indicated with fine lines. This design seamlessly integrates smooth transitions at the blade tips, employing a non-conformal mesh interface to ensure compatibility and continuity within the mesh structure, which is crucial for achieving accurate and reliable simulation results in our research

Table 1 Mesh Statistics for Rotor Blade Row

Mesh Measure	Value	% Bad
(a) For Shroud Tip		
Minimum Face Angle	56.92 [deg]	0
Maximum Face Angle	125.17 [deg]	0
Maximum Aspect Ratio	47.30	0
(b) For Hub		
Minimum Face Angle	54.60 [deg]	0
Maximum Face Angle	116.03 [deg]	0
Maximum Aspect Ratio	36.80	0

Contour Analysis for Blade Design Optimization:

1. Blade Curvature Angle: Figures 8A and 8B demonstrate the Blade Curvature Contour, indicating the curvature distribution across the rotor blade and rotor surfaces.. In Figure 8 (a), the low curvature regions are concentrated near the blade root, where the blade attaches to the rotor hub. This area requires less curvature to maintain structural integrity and aerodynamic efficiency. As we move towards the blade tip, the curvature increases, as shown in Figure 8 (b), which is necessary to manage aerodynamic loading and improve the flow characteristics around the blade's edge.

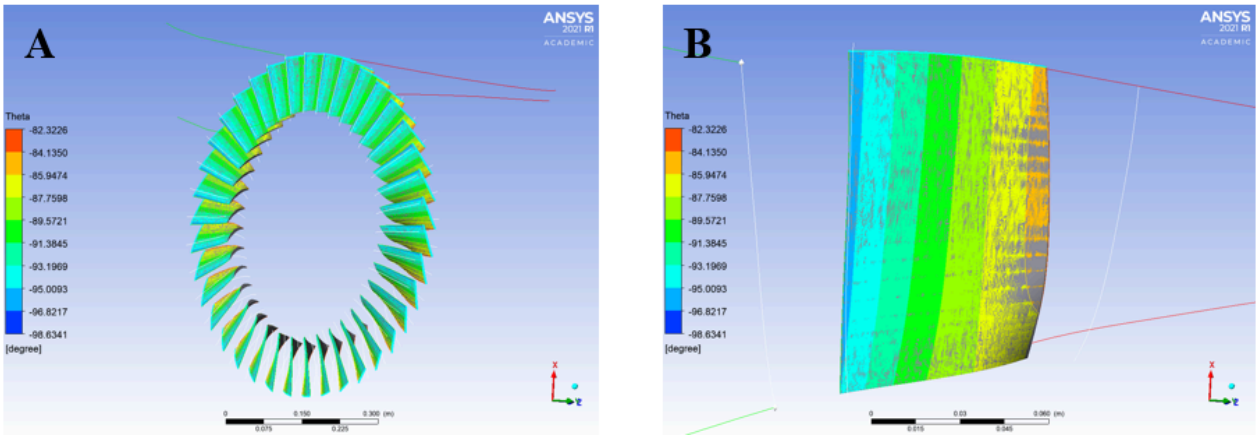

Fig. 8 **A** Blade Curvature Theta Contour on a Rotor Blade. **B** Blade curvature Theta Contours on a Rotor.

2. Minimum Face Angle Contour: Figures 9A and 9B depict the Minimum Face Angle Contour, highlighting mesh quality and the critical minimum face angle for accurate and stable numerical simulations. In Figure 9 (a), low face angle regions are typically found near the blade's leading and trailing edges and at the blade root, indicating areas that may require mesh refinement. In Figure 9B, the minimum face angle contours are shown across the entire blade row, with higher angles desirable as we move outward from the blade root to the tip, enhancing the aerodynamic performance and structural integrity.

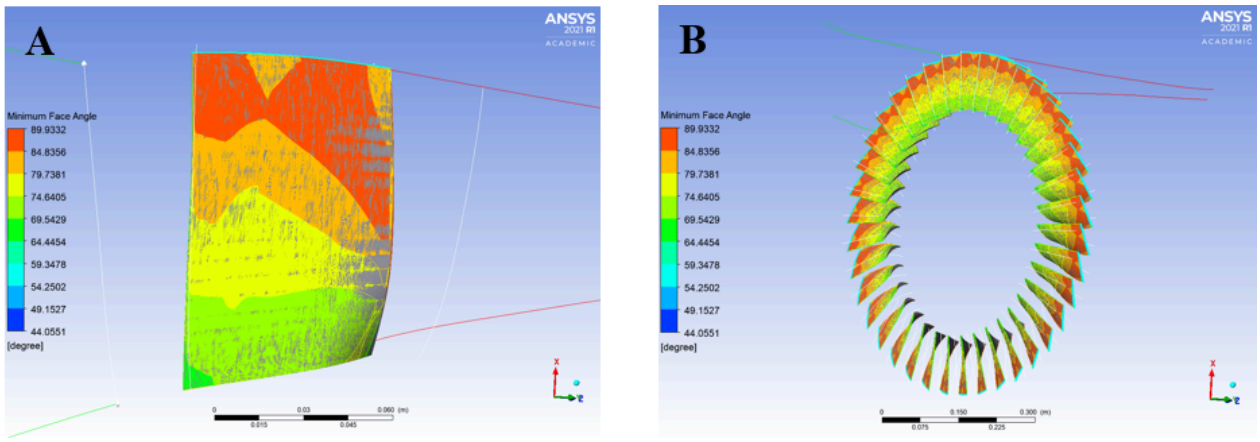

Fig. 9 **A** Minimum Face Angle Contour on Rotor Blade. **B** Minimum Face Angle Contours on a Rotor Blade Row.

Topology Analysis for Blade Design Optimization:

1. Master Topology & Refined Mesh: are critical for accurately capturing the aerodynamic characteristics of the rotor blade. At the shroud tip (Figure 10 (a)), the structured grid is designed to manage complex flow patterns and shear stresses effectively. Similarly, at the hub region (Figure 11 (a)), the refined mesh ensures precise simulation of fluid dynamics near the blade's root. These detailed meshes are essential for maintaining the integrity of the simulations and achieving reliable results.

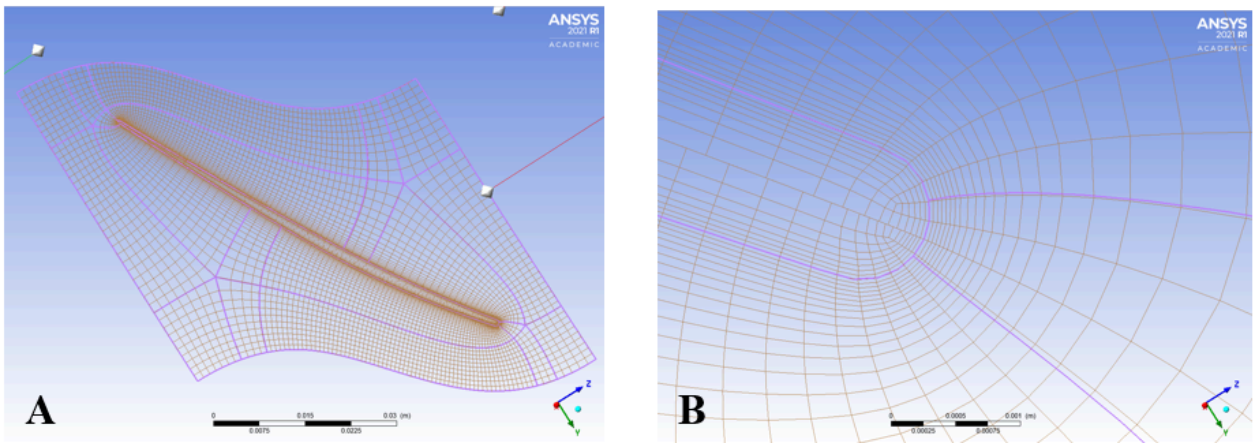

Fig. 10 **A** Master Topology & Refined Mesh at Shroud Tip of a Rotor Blade. **B** Non-conformal mesh interface at Shroud Tip of Rotor Blade.

2. Non-conformal Mesh Interface: The non-conformal mesh interface is crucial for ensuring compatibility and continuity within the mesh structure. At the shroud tip (Figure 11 (b)), this interface facilitates a seamless transition between different mesh segments, preventing numerical errors and enhancing simulation accuracy. In the hub region (Figure 12 (b)), the smooth transition provided by the non-conformal interface is vital for maintaining the quality of the simulation in areas with significant geometric changes.

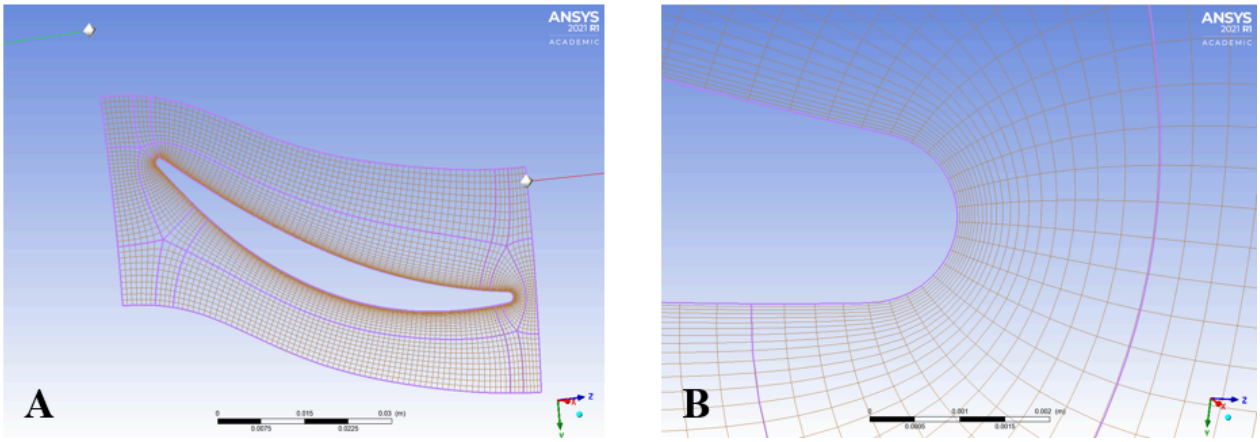

Fig. 11 **A** Master Topology & Refined Mesh at Hub Region of a Rotor Blade. **B** Non-conformal mesh interface at Hub Region of Rotor Blade.

By thoroughly analyzing the topology and mesh quality at critical regions of the rotor blade, we ensure that our simulations accurately represent the physical phenomena within the axial compressor. This detailed mesh analysis leads to more reliable results and informs the optimization of blade design for improved performance and structural integrity.

2.4 CFX Pre

In our effort to understand turbomachinery dynamics, Ansys CFX has been an essential tool to thoroughly explore the aerodynamics, analyzing pressure losses, refining blade designs, and gaining insights into how the compressor behaves. With the help of refined mesh data, we fine-tuned simulation settings specifically for axial compressors within the ‘Turbo Mode’ in Ansys CFX-Pre. To configure the axial compressor’s arrangement we define 21 separate flow sections as presented in Figure 12 dedicated to IGV and the 10 pairs of rotors and stators to match each flow domain with their respective meshes. This alignment results in a comprehensive and realistic model of the system.

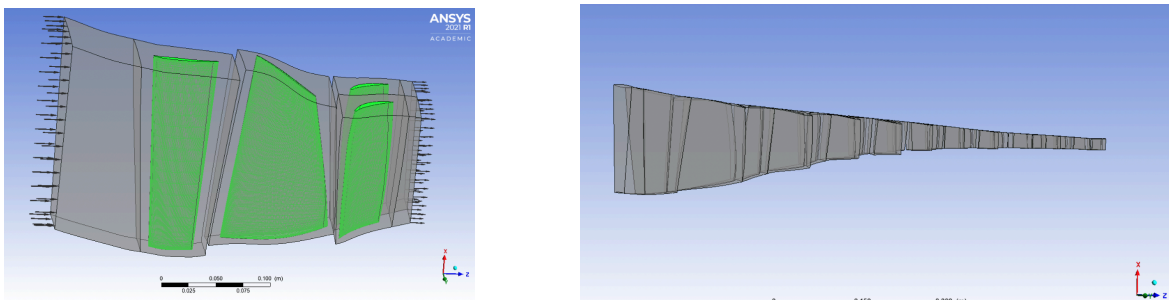

Fig. 12 This image illustrates one stage of the ten-stage compressor on the left, with the inlet guide vane, rotor, and stator highlighted in green. The gray boxes around the blades denote the fluid domain. The right side displays all ten stages assembled in Ansys CFX.

We set initial and boundary conditions to accurately capture the complex flow dynamics. Important factors like pressure and mass flow rate were adjusted to mirror real conditions. The simulation operated at a steady 12000 rpm speed, maintaining a continuous mass flow rate of 64 kg/s, closely resembling real operational settings. This virtual system closely mirrored reality, even reflecting an outlet pressure of around 200 psi. To precisely capture turbulence effects, we opted for the K-omega model within the Reynolds-Averaged Navier-Stokes (RANS) framework[9]. The K-epsilon model is well-suited for high-Reynolds-number flows, such as those in turbomachinery, due to its robustness and reliability in predicting turbulence characteristics. It effectively handles the complex interactions between turbulent eddies and flow structures, ensuring a realistic simulation of the turbulent flow behavior within the compressor. This choice was critical for accurately modeling the intricate fluid dynamics and ensuring the validity of our results in reflecting real-world conditions.

3. Flow Solution

During the actual flow simulation, we employed a parallel run approach utilizing the computational power of 48 cores. Utilizing parallel processing significantly accelerated computation speed and overall efficiency, ensuring timely results. In axial compressor dynamics, achieving solution convergence is pivotal. This marks the point where iterative numerical solutions stabilize, with further steps causing minimal changes. The simulated flow and parameters settle into equilibrium, resembling steady fluid dynamics.

Convergence is a critical reliability indicator, reflecting the alignment of numerical approximations, such as the Navier-Stokes equations, with prescribed conditions and capturing complex flow interactions. In our ANSYS CFD simulations, convergence was evaluated using the residuals of the governing equations, specifically the Navier-Stokes and Euler equations. We set a convergence threshold of 10^{-4} for these residuals, indicating that the iterative process continued until the relative change in the solution from one iteration to the next was less than

10^{-4}. Our simulations achieved this threshold within 300 iterations, demonstrating the robustness and accuracy of our computational approach.

4. Post Processing

During the post-processing phase, our emphasis shifted to data extraction and visualization in Ansys CFD-POST. The visual representation in Figure 13 provides an encompassing insight, showcasing velocity vectors and entropy. The figure shows Mach number contours at the 50% span position. These visualizations are pivotal for unraveling the intricate flow dynamics within the axial compressor. Examining the velocity vectors in Figure 13, a coherent pattern emerges. The velocity vectors provide a clear depiction of the flow direction and intensity within the rotor and stator pairs. The uniformity of the vectors illustrates the continuity of the flow across these components, underscoring the functionality of the axial compressor design.

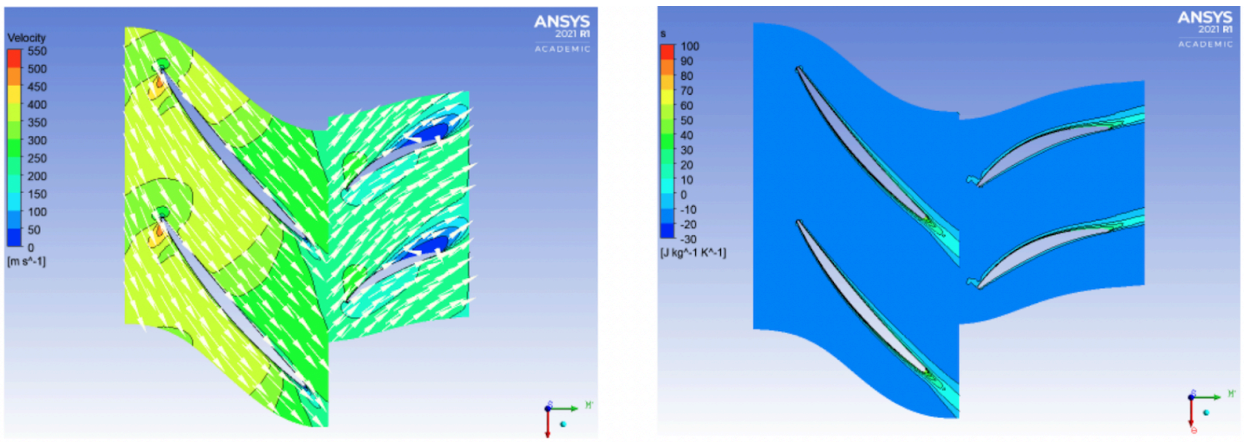

Fig. 13 Velocity Vectors and Entropy Contours at 50% Span.

The entropy contours, notably elevated at the tips, indicate regions of higher entropy generation. This observation implies potential energy losses associated with fluid mixing and diffusion, a common phenomenon in turbomachinery due to blade interactions.

Results

Optimizing all ten stages of the axial compressor simultaneously posed a considerable challenge due to its computational complexity. To streamline the process, we adopted a sequential approach, addressing each stage individually. Our initial objective was to increase the pressure ratios within the first stage of the axial compressor, encompassing the intricate interplay of the inlet guide vane (IGV), Rotor 1 (R1), and Stator 1 (S1). Through a comprehensive parameterization involving mass flow rate, rotor rotational speed, and outlet pressure, we successfully derived optimal conditions tailored to cruise flight scenarios for the axial compressor. The ensuing visual representation showcases the response surface obtained from an array of distinct design points that were executed.

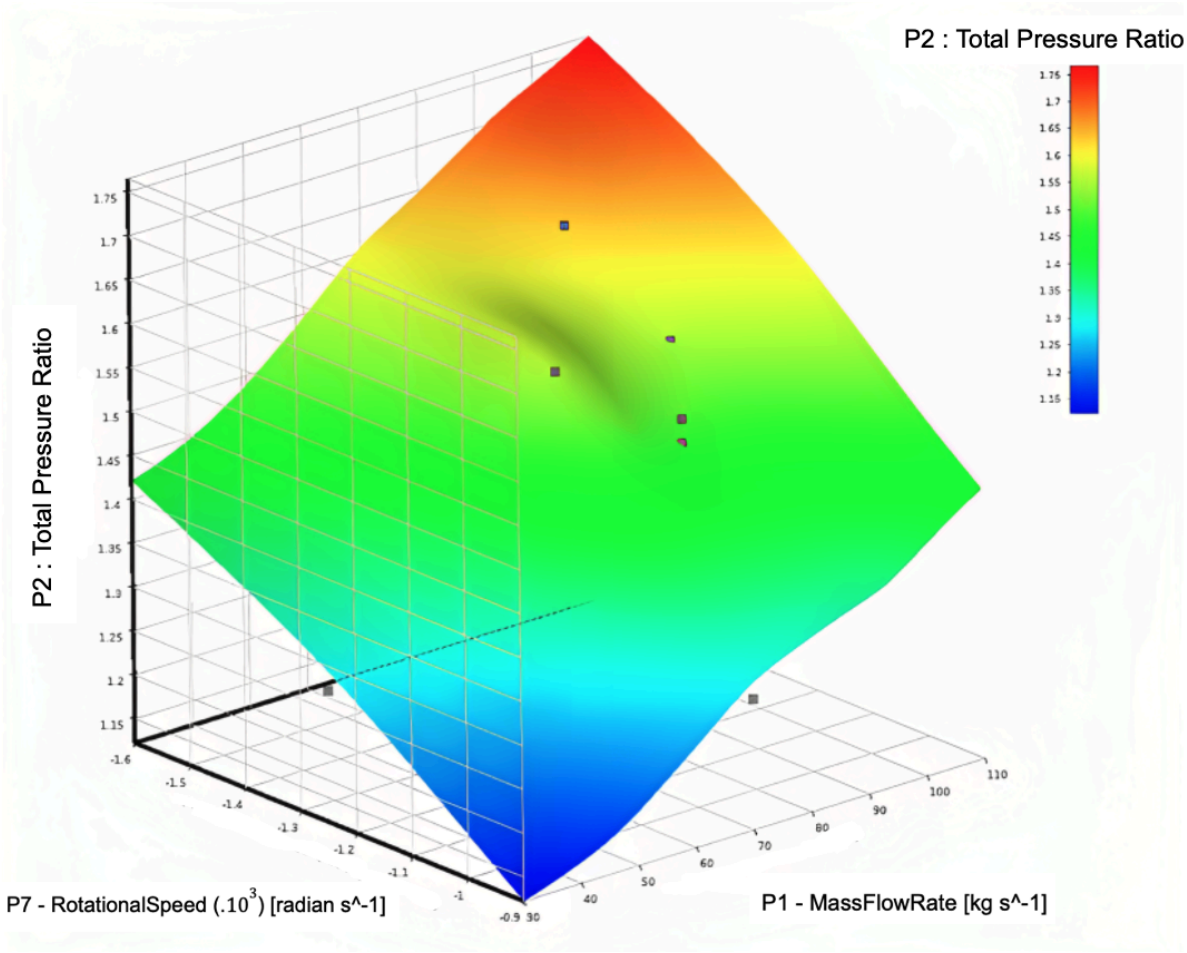

Fig. 14 The generated response surface for an axial compressor stage depicts mass flow rate (x-axis) and rotational speed (y-axis) as input parameters, with the paramount pressure ratio (z-axis) standing as our optimization focal point.

The idea behind conducting an array of design point experiments was to explore the engine's performance boundaries, identifying both its operational strengths and limitations. Leveraging these design points, we crafted a comprehensive compressor map, effectively delineating the extent of our compressor's capabilities. Figure 15 illustrates the surge line and choke line, plotted against varying compressor speeds. The surge line shows the point at which the pressure ratio attains levels that prompt reverse flow within the compressor. Conversely, the choke line denotes the threshold where an excessive mass flow rate overwhelms the compressor, resulting in a sharp efficiency decline and operational failure.

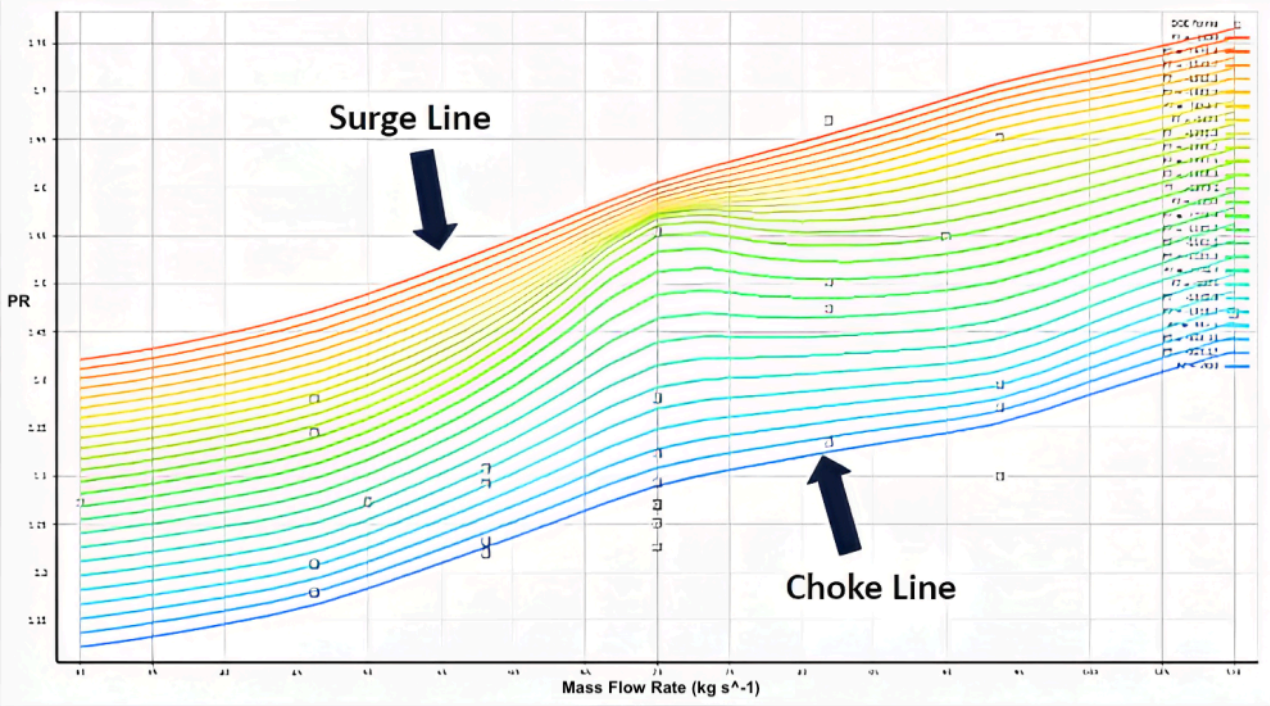

Fig. 15 A compressor map in which the Surge Line and Choke line are represented by the top and bottom lines, respectively.

On understanding airflow dynamics during cruise flight, we analyzed the impact of changes in blade count and the space between the blades and the casing (tip clearance) on compressor performance. Adjusting blade count alters blade solidity, crucially influencing the pressure ratio for the stage. In axial compressors, the initial stages operate at supersonic speeds at the blade tips, making the clearance between blades and casing crucial for turbine efficiency. Managing clearance between blades and casing is vital to mitigate issues like shockwaves, flow separation, and wave drag. Figure 14 shows the outcomes of varying blade count and shroud tip clearance for the first two rotors.

Subsequently, we worked to integrate the outcomes derived from our previous simulations, encompassing both axial compressor conditions and compressor geometry analyses. Leveraging Ansys' optimization tool, we harnessed input parameters to generate potential solutions aligning with our objectives.

Table 2 Optimal Operating Configuration: Results from Simulation Analysis

Parameter	Value
Mass Flow Rate (kg s-1)	41.701
Outlet Pressure (Pa)	200,170
Rotational Speed (radian s-1)	-1382
Total Pressure Ratio	4.2653
Stage 2 Total Pressure Ratio	1.7672
Stage 3 Total Pressure Ratio	1.7307
Stage 4 Total Pressure Ratio	1.2622
Stage 5 Total Pressure Ratio	1.2066
Total Temperature Ratio	1.723
Polytropic Efficiency Out	77.669
Isentropic Efficiency Out	73.061

Analysis and Conclusion

We have successfully achieved a 12.5% increase in the pressure ratio across the initial stages of the rotor. Nevertheless, there remains potential within this project for further enhancement. Notably, a crucial avenue for improving the project's precision would have involved conducting an unsteady simulation. The intricate interplay between the rotor and stator blades inherently manifests as an unsteady phenomenon, and the application of our current steady-state mixing plane model does not fully resolve the physics of the problem.

Of particular significance is the incapability of the steady-state model to accurately represent shockwaves, especially those arising at supersonic Mach numbers. As illustrated in Figure 16, our observations indicate elevated Mach numbers at the tips of the rotor blades, which could potentially give rise to shockwave formations.

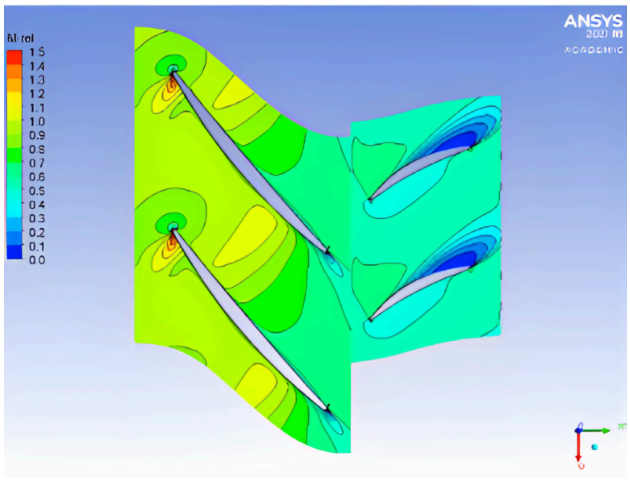

Fig. 16 Mach Number Contours at 50% Span for a Blade Passage of a Rotor and Stator Stage.

An additional aspect that could have been incorporated into our modeling pertains to the inclusion of bleed valves. Upon examination Figure 16, it becomes evident that the gaps situated between the 5th and 7th stages serve as channels for the placement of bleed valves. The absence of these essential components had a large impact on the outcomes yielded by our comprehensive ten-stage simulations. This omission significantly influenced our decision to concentrate solely on optimizing the initial four stages of the compressor.

Furthermore, our simulation could have also encompassed the intricate dynamics of the film cooling layer enveloping the rotor blades. This protective film cooling layer shown in Figure 17, composed of a blend of oil and air, serves the crucial purpose of averting overheating and potential melting of the compressor blades. Given the elevated temperatures and pressures inherent to combustion processes, the durability of these blades can sometimes dictate the permissible operational limits. As elucidated in the introduction, ongoing experimentation with novel carbon fiber materials aims to fortify the blades against high temperatures, thereby ensuring resilience and longevity within the compressor's operational realm.

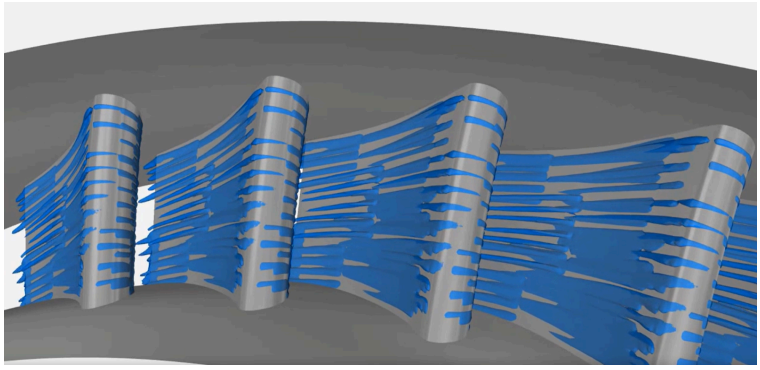

Fig. 17 Film Cooling Layer for a Turbine Blade Following the Combustion Process[5].

With our newfound tools for modeling the axial compressor, we have the opportunity to extend our expertise to encompass additional engine components, culminating in a comprehensive module simulation. This expansion entails simulating not only the combustion process but also the intricate dynamics of the turbine blades. By doing so, we can propel our efforts towards enhancing engine efficiency, all the while gaining the ability to visually assess the impact of the optimized compressor on thrust generation.

Our research progress was primarily hindered by the challenge of connecting our project to the university's supercomputer. At UCSD, we have access to the EXPANSE supercomputer, which has the potential to run our design points on a much larger scale compared to the limited computational resources available in our on-campus CFD lab. With approximately 48 cores at our disposal in the CFD lab, we were constrained to running only about 30 design points. While this allowed for some optimization, being connected to the supercomputer could have enabled us to process thousands of design points in just a single day. In our future research we will incorporate the supercomputer with our research.

Acknowledgments

We wish to express our sincere appreciation to the Undergraduate Research Hub's TRELS program and its coordinator, Daniel Movahed, for sponsoring our research. We are thankful to Professor Oliver T. Schmidt for supporting our research project. We extend special thanks to PhD student Edward Lowell for his invaluable guidance, unwavering support, and help with the Undergraduate Computational Modelling & Flow Physics Lab resources. We also extend our gratitude to the San Diego SuperComputer for generously allocating 200,000 ACCESS credits to support our project (ENG230006).

Appendix

Appx. 1 Circumferential Blade Count for Each Blade Row in the High Pressure Compressor

Blade Row	Circumferential Blade Count
HPC Blade 1	32
HPC Blade 2	28
HPC Blade 3	50
HPC Blade 4	38
HPC Blade 5	50
HPC Blade 6	68

HPC Blade 7	82
HPC Blade 8	60
HPC Blade 9	92
HPC Blade 10	70
HPC Blade 11	110
HPC Blade 12	80
HPC Blade 13	120
HPC Blade 14	82
HPC Blade 15	112
HPC Blade 16	84
HPC Blade 17	104
HPC Blade 18	88
HPC Blade 19	118
HPC Blade 20	96
HPC Blade 21	140

References

1. Holloway, P., Knight, G., Koch, C., and Shaffer, S. "Energy Efficient Engine High Pressure Compressor Detail Design Report." NASA Technical Report CR-165558. NASA, May 1982. https://ntrs.nasa.gov/api/citations/19850002690/downloads/19850002690.pdf.

2. Sánchez, A. L. "An Introduction to Compressible Flow for Propulsion Applications." 2023. PDF notes. https://www.coursehero.com/file/189485720/Compressible/.

3. Claus, Russell W., Tim Beach, Siddappaji K., and Hendricks, E. S. "Geometry and Simulation Results for a Gas Turbine." AIAA Journal 24, no. 11 (2015): 1872-1873. https://doi.org/10.2514/3.13046.

4. Ansys, Inc. Ansys TurboGrid User's Guide. 2021. https://path-to-your-pdf-file/Ansys_TurboGrid_Users_Guide.pdf.

5. Ansys, Inc. "Design and Maintain Turbomachinery." Accessed September 11, 2024. https://www.ansys.com/blog/design-and-maintain-turbomachinery.

6. Ritchie, Hannah. "How Much Does Aviation Contribute to Climate Change? How Will This Change in the Future?" Accessed September 11, 2024. www.sustainabilitybynumbers.com/p/aviation-climate-part-one#:~:text=Aviation%20is%20responsible%20for%202.8.

7. "GE's Next-Generation Composite Turbine Blades to Improve Aircraft Fuel Efficiency." New Atlas, September 5, 2014. Accessed February 20, 2024. https://newatlas.com/ge-fan-composite-ge9x/33611/#:~:text=GE%20is%20looking%20to%2a.

8. U.S. Federal Aviation Administration. Airplane Flying Handbook. FAA-8083-3A. Washington, D.C.: U.S. Government Printing Office, 2004.

9. "ANSYS FLUENT 12.0 Theory Guide - 4.5.1 Standard - Model." Enea.it, 2021. https://www.afs.enea.it/project/neptunius/docs/fluent/html/th/node66.htm.